Geochimica et Cosmochimica Acta, Vol. 69, No. 23, pp. 5557–5566, 2005

0016-7037/05 $30.00 + .00

doi:10.1016/j.gca.2005.07.020

Solution mechanisms of H_2O in depolymerized peralkaline melts

BJORN O. MYSEN* and GEORGE D. CODY

Geophysical Laboratory, Carnegie Institution of Washington, 5251 Broad Branch Road NW, Washington DC 20015, USA

(*Received March* 8, 2005; *accepted in revised form July* 18, 2005)

Abstract—Solubility mechanisms of water in depolymerized silicate melts quenched from high temperature (1000°–1300°C) at high pressure (0.8–2.0 GPa) have been examined in peralkaline melts in the system Na_2O-SiO_2-H_2O with Raman and NMR spectroscopy. The Na/Si ratio of the melts ranged from 0.25 to 1. Water contents were varied from ~3 mol% and ~40 mol% (based on O = 1). Solution of water results in melt depolymerization where the rate of depolymerization with water content, $\partial(NBO/Si)/\partial X_{H2O}$, decreases with increasing total water content. At low water contents, the influence of H_2O on the melt structure resembles that of adding alkali oxide. In water-rich melts, alkali oxides are more efficient melt depolymerizers than water. In highly polymerized melts, Si-OH bonds are formed by water reacting with bridging oxygen in Q^4-species to form Q^3 and Q^2 species. In less polymerized melts, Si-OH bonds are formed when bridging oxygen in Q^3-species react with water to form Q^2-species. In addition, the presence of Na-OH complexes is inferred. Their importance appears to increase with Na/Si. This apparent increase in importance of Na-OH complexes with increasing Na/Si (which causes increasing degree of depolymerization of the anhydrous silicate melt) suggests that water is a less efficient depolymerizer of silicate melts, the more depolymerized the melt. This conclusion is consistent with recently published ^1H and ^{29}Si MAS NMR and ^1H-^{29}Si cross polarization NMR data.

1. INTRODUCTION

Characterization of solution mechanisms of water in silicate melts is central to modeling the physics and chemistry of rock-forming processes in the interior of the Earth and terrestrial planets because of the strong effects of water on properties of silicate melts at high pressures and temperatures. Not all effects of water on melt properties and structure are, however, known. These include the extent to which melt properties of hydrous systems depend on silicate melt composition (e. g., Watson, 1994) and water content (e. g., Chekhmir et al., 1988; Zhang et al., 1991; Hess and Dingwell, 1996).

Experimental data on water solution mechanisms, which are needed to describe property behavior, are for the most part limited to highly polymerized melts where most solution models suggests that water breaks up the structure (e.g., Wasserburg, 1957; Burnham, 1975; Farnan et al., 1987). This break-up may be accomplished, for example, by reacting bridging oxygen with H_2O to form Si-OH complexes as in a simple melt system such as SiO_2-H_2O (Moulson and Roberts, 1961; Stolen and Walrafen, 1976; McMillan and Remmele, 1986; Farnan et al., 1987). In aluminosilicate melts, interaction between water, metals, and alumina can create charge-imbalance of Al^{3+} in tetrahedral coordination. That charge-imbalance may lead to formation of nonbridging oxygen (e.g., Mysen and Virgo, 1986), although such a structural model is not universally accepted (Kohn et al., 1992; Schmidt et al., 2001; Padro et al., 2003).

For depolymerized melts, there is the potential for additional complexity with competing water solution mechanisms that may include both the silicate network and network-modifying cations. Results from ^{29}Si MAS NMR and CP MAS NMR spectroscopy of $Na_2Si_4O_9$-H_2O glasses indicate silicate depolymerization (Kümmerlen et al., 1992; Schaller and Sebald, 1995; Zotov and Keppler, 1998; Cody et al., 2005). Recent NMR data of Ca,Mg-silicate melts suggest, however, that Ca-OH and Mg-OH complexing are formed (Xue and Kanzaki, 2004). This conclusion is consistent with an earlier Raman spectroscopic study of melts in the $Ca(OH)_2$-SiO_2 and NaOH-SiO_2 systems where Mysen and Virgo (1986) proposed that Ca-OH and Na-OH complexing could be important. Such a mechanism could induce the silicate structure to polymerize because in this process network-modifying alkali metals or alkaline earths are scavenged from the silicate to form OH-complexes.

The question is, therefore, even for hydrous binary metal oxide-silica melts (i) how important is the formation of OH-groups with alkalis or alkaline earths relative to Si-OH complexing, and (ii) how are individual Q^n-species in the melts involved in the water solution processes? To answer these questions, we have conducted a series of Raman- and NMR-based structural studies of H_2O solubility mechanisms in sodium silicate melts as a function of degree of polymerization of the silicate (sodium/silicon ratio) and water content. Some of the NMR results can be found in Cody et al. (2005). Those data will be used in conjunction with additional NMR and Raman data to shed new light on these issues.

2. EXPERIMENTAL METHODS

Starting compositions were on the join Na_2O-SiO_2-H_2O with H_2O contents ranging from ~3 to ~40 mol% [based on number of oxygen (O) = 1]. Six compositions were used with nominal NBO/Si of the anhydrous glasses and melts between 0.25 and 1 (Fig. 1). Some of these samples are the same as those used by Mysen and Cody (2004) for H_2O solubility measurements in the 0.8–2.0 GPa and 1000°–1400°C pressure and temperature range, respectively.

Anhydrous Na-bearing starting glasses were made by mixing spectroscopically pure Na_2CO_3 and SiO_2, ground under alcohol for ~1 h,

* Author to whom correspondence should be addressed (b.mysen@gl.ciw.edu).

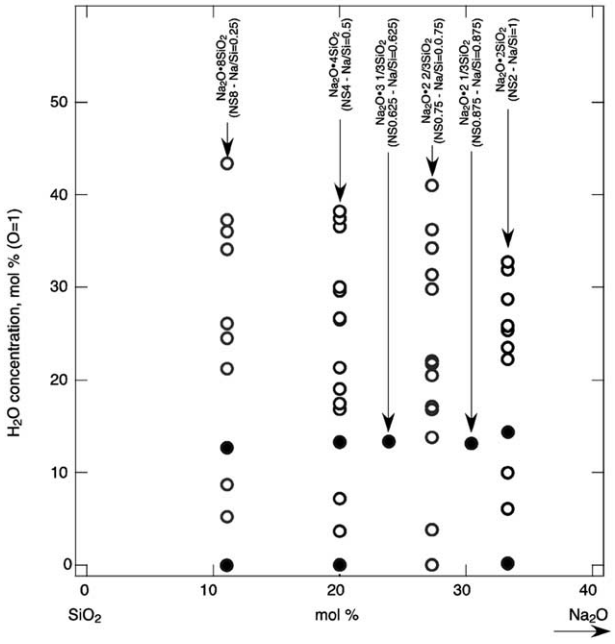

Fig. 1. Composition of starting materials and water contents of samples analyzed with Raman and NMR studies. Solid symbols: sample used for ^{29}Si MAS NMR and Raman spectroscopy. Open symbols: sample used for Raman spectroscopy.

decarbonated during slow heating (~1.5°C/min), and then melted at ~100°C above their liquidus temperatures at 0.1 MPa (liquidus data from Osborn and Muan, 1960) for 60 min. The samples were then quenched to glass by cooling the outside of the sample container in liquid H_2O. This glass starting was crushed to ~20 μm grain size and stored at ~250°C when not in use to avoid reaction between the glass starting material and moisture from ambient air.

Hydrous glasses were prepared at high pressure (0.8–2.0 GPa) and high temperature (1000°–1300°C) in the solid-media, high-pressure apparatus (Boyd and England, 1960). The samples were contained in Pt capsules that were welded shut and subjected to experimental conditions in 0.75"-diameter furnace assemblies based on the design of Kushiro (1976). Temperatures were measured with Pt-Pt90Rh10 thermocouples with no correction for pressure on their emf, which may be as much as ±10°C (Mao et al., 1971). Pressure was calibrated against the melting point of NaCl and the calcite-aragonite transformation (Bohlen, 1984). Estimated uncertainties are ±10°C and ±0.1 GPa, respectively.

The powdered starting glasses were loaded together with double-distilled, deionized H_2O (1.0–2.5 μL depending on desired H_2O content) into 3 mm outside diameter (OD) by 7 mm long or 5 mm OD by 10 mm long Pt containers and welded shut. Water was injected using a microsyringe with 0.1 μL precision. The exact amount of H_2O added was, however, determined by weighing. The weighing accuracy is ±0.02 mg. Reported H_2O contents of the experimental charges are accurate to ±2% or better (2% for the lowest H_2O contents).

The hydrous glasses could not analyzed with instrumental methods because the glasses in many of these samples, in particular those from experiments with high water contents (>10 wt%), contained finely distributed bubbles that probably exsolved during quenching (see also Mysen and Wheeler, 2000, for additional detail). Therefore, analysis of the H_2O contents of the glasses by instrumental techniques was unreliable because it is not possible to account for H_2O lost by exsolution of H_2O from the melt during temperature-quenching of the hydrous melt to a hydrous glass. Instead, the water solubility in the samples examined here was determined by chemographic techniques as reported by Mysen and Cody (2004).

The H_2O solubility behavior in the melts was examined with Raman and NMR spectroscopy. Spectroscopic measurements were conducted on glasses that were temperature-quenched under isobaric conditions (quenching rate ~ 100°C/s). Because of the hygroscopic nature of these glasses as well as the tendency of, in particular, the most sodic glass to exsolve H_2O and to undergo incipient crystallization within days after formation, spectroscopic measurements were carried out immediately following quenching of a high-pressure experiment. For Raman spectroscopy, spectra were recorded within ~10 min after opening the sample containers. For NMR measurements, ~30 min elapsed between extracting the samples from the containers and having the crushed powder spinning in dry air in the NMR rotor.

Nuclear magnetic resonance (NMR) experiments were conducted only on samples where there was no evidence of exsolution of H_2O upon quenching and before incipient crystallization begun. We found that samples with ~7.5 wt% H_2O or less met these requirements. Raman measurements, using micro-Raman techniques, were also conducted with samples with higher water contents. This was accomplished by positioning the ~1 μm diameter laser beam on areas of glass away from bubbles.

Raman spectra were recorded with a Dilor XY confocal micro-Raman spectrometer using the 514 nm line of an Ar^+ ion laser for sample excitation. The laser power was several hundred mW at the sample. The Raman system was equipped with a cryogenic Thompson Model 4000 CCD (charge-coupled detector) for signal detection. Acquisition time was typically 60 s/CCD window, and two windows were needed to record the frequency region of first-order Si-O Raman scattering.

Most of the solid state nuclear magnetic resonance spectroscopy data were reported by Cody et al. (2005). Those data include single pulse ^{1}H and ^{29}Si MAS NMR and ^{1}H-^{29}Si cross polarization experiments. Here, we will address only ^{29}Si single pulse data as these pertain to Q^n-speciation in hydrous glasses and otherwise refer to Cody et al. (2005) for other relevant information.

The NMR data were obtained with a Chemagnetics CMX Infinity 300 Solid State NMR. The static field strength of the magnet is 7.05 T. The Larmor frequency of ^{29}Si at this field is 59 MHz. Single-pulse ^{29}Si MAS NMR spectra (SPMAS) ($\omega_r/2\infty$ = 4 kHz) were obtained by employing ^{29}Si pulse widths corresponding to 30° tip angles, a recycle delay of 100 s, and 1000 acquisitions.

3. RESULTS

3.1. ^{29}Si-NMR

The single-pulse ^{29}Si MAS NMR (SPMAS) spectra of hydrous (7.6–7.7 wt% H_2O) and anhydrous glasses were used to extract information on Q^n-speciation. These spectra were fitted to gaussian lines (Fig. 2) with the relative areas of the absorption bands given in Table 1.

The SPMAS ^{29}Si spectra of the anhydrous glasses are nearly identical to existing spectra of similar compositions (e. g., Maekawa et al., 1991; Buckermann et al., 1992) with resonances near −80, −90, and −110 ppm assigned to Q^2, Q^3, and Q^4 structural units. The absorption near −80 ppm is not observed in the spectra of the most polymerized, anhydrous samples, NS4 and NS8. These spectra will not discussed further here as these have been described and discussed in detail in existing literature (Maekawa et al., 1991; Buckermann et al., 1992).

The spectra of the Na_2O-SiO_2 + 7.6–7.7 wt% H_2O glasses comprise the same peaks, but with different intensities. The peak near −94 ppm generally becomes more intense and that near −107 ppm diminishes in intensity in the spectra of hydrous glass (Fig. 2; Table 1). These two peaks are assigned to Q^4 and Q^3 structural units, respectively (e.g., Engelhardt and Michel, 1987; Stebbins, 1987; Maekawa et al., 1991; Kümmerlen et al., 1992).

In contrast to the NMR spectra of anhydrous NS4 and NS8

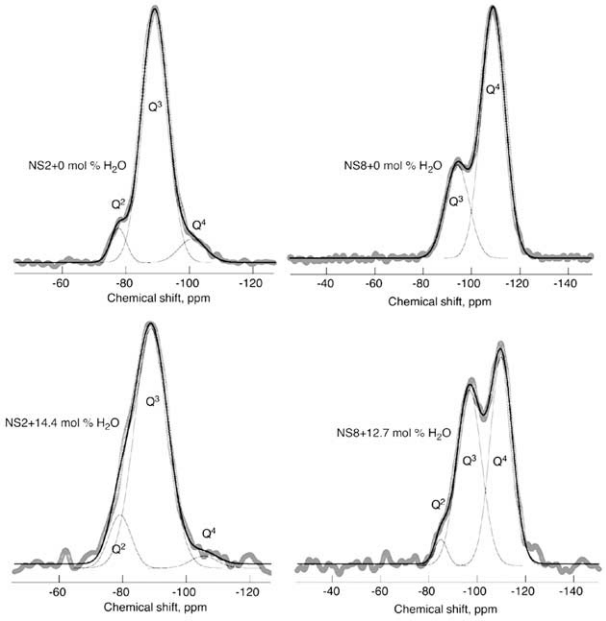

Fig. 2. Examples of curve-fitted ^{29}Si MAS NMR spectra of compositions indicated.

glass, the ^{29}Si-NMR spectra of the hydrous NS4 and NS8 glasses also show intensity near −80 ppm, consistent with Q^2 species in the hydrous glasses (e.g., Engelhardt and Michel, 1987; Stebbins, 1987; Maekawa et al., 1991; Kümmerlen et al., 1992). For the less polymerized glasses, peaks assigned to Q^2, Q^3, and Q^4 occur in spectra of both anhydrous and hydrous glasses. Their relative intensities depend on the water content (Table 1). With the exception of NS2 + 7.7 wt% H_2O, the integrated intensity of the band assigned to Q^4 in the spectra of hydrous glasses decreases relative to the intensity in the spectrum of the anhydrous equivalent glass. In NS2 + 7.7 wt% H_2O, the integrated intensity of this band actually increases (Table 1). The intensity of the absorption band assigned to Q^2 is positively correlated with water content, whereas the intensity of the absorption assigned to Q^3 is relatively insensitive to water content in NS2 and NS2 2/3 glasses and increases in hydrous (7.6 wt% H_2O) NS4 and NS8 glass relative to their anhydrous equivalents at least to 7.6–7.7 wt% H_2O.

The Q^n-species abundance evolution as a function of bulk melt NBO/Si of the anhydrous Na_2O-SiO_2 and hydrous Na_2O-SiO_2 with 7.6–7.7 wt% H_2O glasses resembles one another with a Q^3-abundance maximum for bulk melt NBO/Si near 1 (Fig. 3).[1] There is a decay in Q^4 and an increase in Q^2 abundance with increasing NBO/Si. In other words, the overall topology of the Q^n abundance trends with NBO/Si of anhydrous Na_2O-SiO_2 and hydrous Na_2O-SiO_2-H_2O glasses with approximately the same H_2O content resemble one another. This observation leads to the suggestion that dissolved H_2O affects the Q^n abundance population in a manner that is qualitatively similar to the effect of Na_2O.

The Q^n abundance from the ^{29}Si MAS NMR spectra of anhydrous and hydrous (7.6–7.7 wt% H_2O) glasses differs in detail, however, in that the Q^3 concentration in the Na_2O-SiO_2-H_2O glasses is lower (Fig. 3). The Q^4 and Q^2 concentrations are shifted to slightly higher values compared with the anhydrous glasses (Fig. 3). These relations may suggest that Na^+ and H^+ bond preferentially to different nonbridging oxygen in the melts. Sodium probably is bonded predominantly to nonbridging oxygen in Q^3 species, whereas H^+ shows a preference for nonbridging oxygen in Q^2 species. Thus, increasing H^+/Na^+ results in a decrease in the Q^3/Q^2 abundance ratio. Mass-balance requires an increase in Q^4 abundance as well.

An examination of the Q^n-abundance population as a function of melt NBO/Si in the binary systems K_2O-SiO_2, Na_2O-SiO_2, and Li_2O-SiO_2 (Maekawa et al., 1991) may shed further light on preference of metal cations for nonbridging oxygen in different Q^n species. In the latter three systems, the Q^n abundance variations with the NBO/Si of the melt resemble one another (Fig. 3). However, as the ionic radius of the alkali metal decreases, the Q^3/Q^2 abundance ratio decreases. This is because the smaller the ionic radius of the alkali, the greater is its tendency to form bonding with nonbridging oxygen in Q^2-species relative to bonding with nonbridging oxygen in Q^3-species (Mysen, 2003). Mass-balance requires an increased abundance of Q^4 species as that of Q^2 species increases as observed. This trend is analogous to seen when H^+ is added to Na-silicate melts.

Addition of H_2O to Na_2O-SiO_2 melts results in Q^n-abundance trends with bulk melt NBO/Si between those observed in the anhydrous Na_2O-SiO_2 and Li_2O-SiO_2 systems (Fig. 3).

[1] The NBO/Si-values are calculated from the Q^n-species abundance data in Table 1.

Table 1. Species abundance (mol %) in hydrous and anhydrous Na_2O-SiO_2-H_2O glasses from ^{29}Si MAS NMR (data for hydrous glasses from Cody et al., 2005).

Composition	Na/Si	H_2O (wt %)	Q^4	Q^3	Q^2	Q^1
NS2	1.00	0.0	6.8 ± 0.3	85.2 ± 0.2	8.0 ± 0.1	0.0
NS2	1.00	7.7	13.1 ± 0.6	68.7 ± 0.5	16.5 ± 0.4	1.7 ± 1.0
NS0.875	0.87	7.7	10.4 ± 0.7	67.9 ± 0.5	17.8 ± 0.5	3.9 ± 0.9
NS2 2/3	0.74	0.0	27.4 ± 0.9	69.8 ± 0.7	2.9 ± 0.5	0.0
NS2 2/3	0.74	7.6	12.9 ± 1.0	68.2 ± 0.7	15.6 ± 0.7	3.4 ± 1.0
NS0.625	0.62	7.6	23.7 ± 0.9	63.7 ± 0.8	10.0 ± 0.6	2.5 ± 1.0
NS4	0.5	0.0	51.9 ± 0.1	48.1 ± 0.1	0.0	0.0
NS4	0.5	7.6	28.5 ± 1.3	59.3 ± 1.0	11.7 ± 0.6	0.6 ± 0.6
NS8	0.25	0.0	73.8 ± 0.7	26.2 ± 0.7	0.0	0.0
NS8	0.25	7.6	54.6 ± 0.3	37.6 ± 0.3	7.8 ± 0.6	0.0

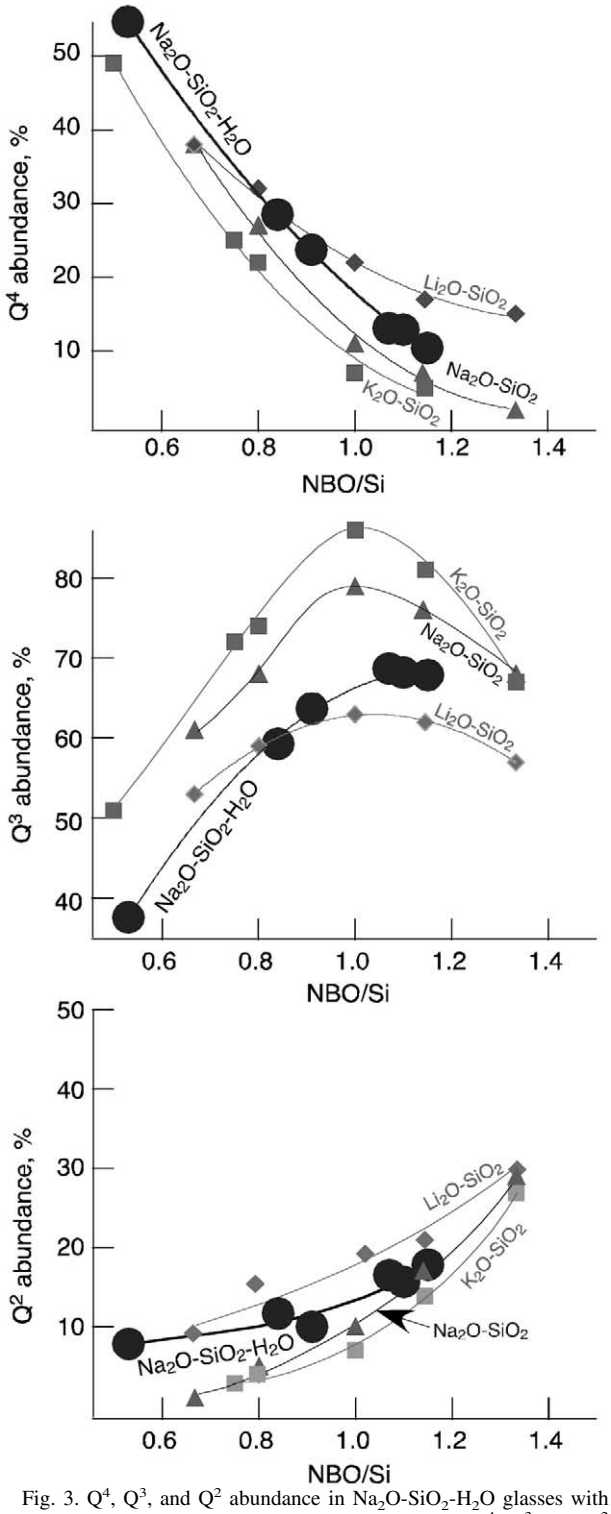

Fig. 3. Q^4, Q^3, and Q^2 abundance in Na_2O-SiO_2-H_2O glasses with 7.6–7.7 wt% H_2O (see Table 1). Also shown is the Q^4, Q^3, and Q^2 abundance in anhydrous Li_2O-SiO_2, Na_2O-SiO_2 and K_2O-SiO_2 glasses from Maekawa et al. (1991). The lines through the data points are drawn to guide the eye.

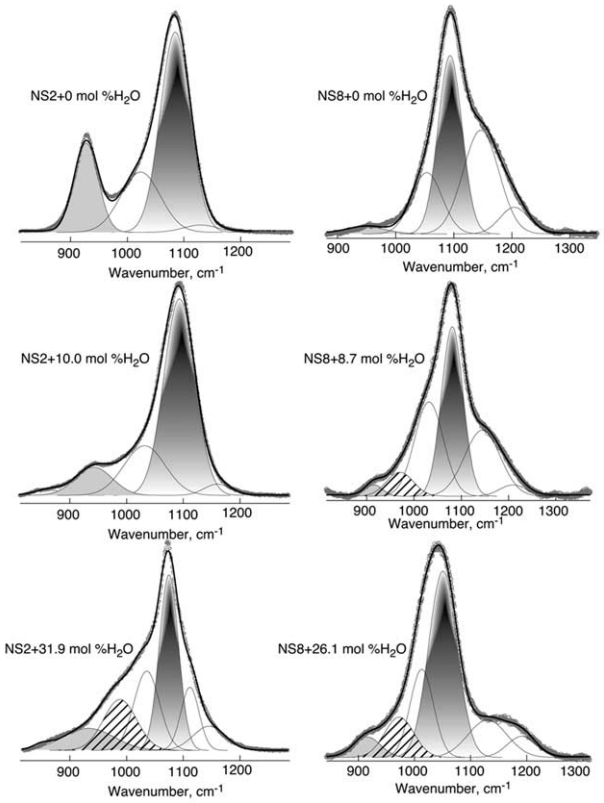

Fig. 4. Examples of curve-fitted Raman spectra. Mol% H_2O calculated on the basis of O = 1.

When considering these relationships, it should be remembered that in the Na_2O-SiO_2-H_2O system, as in other melts, most likely water is dissolved both in the form of molecular H_2O (which will have no effect on the Q^n-distribution) and as OH (e.g., Stolper, 1982; Silver et al., 1990; Nowak and Behrens, 1995; Zotov and Keppler, 1998; Sowerby and Keppler, 1999). In the system Na_2O-SiO_2-H_2O, this H^+ (the proportion forming OH groups in the melt) and Na^+ compete for nonbridging oxygen and the Q^n-population evolution with bulk melt NBO/Si reflects this competition.

3.2. Raman Spectroscopy

The portion of the Raman spectra most relevant to Q^n-abundance is the high-frequency regime between ~850 and 1250 cm^{-1} (Brawer and White, 1975; McMillan and Wolf, 1995; Mysen, 1995). Only this portion of the spectra will be discussed because melt polymerization and Q^n-abundance populations are the focus of this study.

Examples of spectra in this frequency regime for NS2 and NS8 samples are shown in Figure 4.[2] The spectra were fitted to 4–6 gaussian bands after correction for instrumental background and temperature-dependent Raman scattering intensity (in this case, 25°C) (Long, 1977). The curve-fitting was carried out with the IGOR software package from Wavemetrics. In

[2] The line parameters from deconvolution of all the Raman spectra are available from the author upon request.

these fits, position (Raman shift), bandwidth, and band intensity were treated as independent variables and minimum χ^2 was used as the principal convergence criterion.

The band near 950 cm^{-1} (marked with grey in Fig. 4) is assigned to Si-O^- stretch vibrations in Q^2-species, an interpretation consistent with Raman spectra of other metal oxide silicate glasses (e.g., Brawer and White, 1975; Furukawa et al., 1981; Mysen et al., 1982; McMillan, 1984) and also consistent with the ^{29}Si-NMR spectra of these glasses (Fig. 2, Table 1). The band near 1100 cm^{-1} (gradient-filled grey) is assigned to Si-O^- stretch vibrations in Q^3-species consistent with Raman spectra of other metal oxide silicate glasses (e.g., Brawer and White, 1975; Furukawa et al., 1981; Mysen et al., 1982; McMillan, 1984) and also with the ^{29}Si-NMR spectra (Fig. 2, Table 1). The two bands near 1150 and 1200 cm^{-1}, respectively, in the spectra of anhydrous and hydrous NS8 in Figure 4 are both assigned to Si-O stretching in fully polymerized Q^4 units. With increasing Na/Si these two bands merge into a single band centered near 1150 cm^{-1} as seen, for example, in the spectra of anhydrous and hydrous NS2 in Figure 4. This latter spectral evolution with metal/silicon ratio is the same as that seen in Raman spectra of other alkali and alkaline earth silicate glasses and melts (Mysen et al., 1982; Mysen and Frantz, 1994).

The 1050 cm^{-1} band fitted to all the spectra also has been reported in Raman spectra of vitreous silica as well as in Raman spectra of other alkali and alkaline earth silicate and aluminosilicate melts and glasses (e.g., Bell and Dean, 1972; Brawer and White, 1975, 1977; Furukawa et al., 1981; Mysen et al., 1982; Fukumi et al., 1990; McMillan et al., 1992). This band remains in spectra of glasses with compositions ranging from less polymerized than pyrosilicate (NBO/Si $\geq$3) to pure SiO_2 (Mysen et al., 1982). This band has been assigned to Si-O^o vibrations in any structural unit that contains bridging oxygen, but does not need by itself be fully polymerized (Lasaga, 1982) or to Si-O vibrations in Q^3-species associated with alkali metals or alkaline earths (Fukumi et al., 1990; McMillan et al., 1992). If this latter assignment were correct, spectra of CaO-SiO_2 and (Ca,Mg)O-SiO_2 glasses in the bulk NBO/Si-range between ~1 and 3.95, which all have the 1050 cm^{-1} band (Mysen et al., 1982), would suggest that Q^3 species is important in all of these glasses. Silicon-29 MAS NMR spectra of alkali silicate glasses indicate, however, that Q^3-abundance is below the detection limits in glasses whose bulk NBO/Si is between 1 and 2 (Maekawa et al., 1991). The Q^n-speciation in alkali and alkaline earth silicate glasses resemble each other with the main difference being that for glasses with fixed bulk NBO/Si, the Q^3 abundance is less in alkaline earth than in alkali silicate glasses (see also Stebbins, 1995, and references therein). Thus, it is quite unlikely that the 1050 cm^{-1} band in any of these glasses can be assigned to Q^3 species. Finally, we also note that there is no evidence for a second Q^3 structural unit in the ^{29}Si-NMR spectra of anhydrous glasses reported here or existing in the literature (e.g., Maekawa et al., 1991; Buckermann et al., 1992). The former assignment (Si-O° vibration) is, therefore, the more likely of the two alternatives.

Finally, nearly all the spectra of hydrous glasses have a band between 970 and 1000 cm^{-1} (hatched in the examples in Fig. 4). As illustrated with the relationship between χ^2 and whether or not a band in the 970–1000 cm^{-1} is included in the fit (Table 2), from a statistical point of view, the fits are better when this band is included. In light of the ^{29}Si MAS NMR spectra suggesting Q^2-species in the hydrous glass (Fig. 2), the interpretation of the ^{1}H MAS NMR data suggesting the presence of Si-OH bonds (Cody et al., 2005), and the commonly reported band near 970 cm^{-1} in the Raman spectra of SiO_2-H_2O glasses where it has been assigned to Si-OH vibrations (e. g., Revesz and Walrafen, 1983; McMillan and Remmele, 1986; Mysen and Virgo, 1986), we assign the band in the 970–1000 cm^{-1} range to Si-OH vibrations. This band cannot, however, be fitted with any confidence to spectra of hydrous NS2 glass with the lowest H_2O contents. Whether this is because it does not exist or whether it is within the precision of the deconvolution procedure cannot be determined.

Table 2. Comparison of χ^2 from fits to hydrous NS4 glasses.

H_2O (wt%)	χ^2 w/970 cm^{-1} band	χ^2 wo/970 cm^{-1} band
2	1026	1859
4	1661	2224
5	166	2225
7.7	846	8697

3.3. Water Solution Mechanisms

The Raman and NMR data are consistent with depolymerization of alkali silicate melts upon solution of water at high pressure and temperature. The ^{29}Si MAS NMR data, furthermore, suggest that the extent to which water causes silicate melt depolymerization diminishes as the Na/Si increases (Table 1). The extent of depolymerization also depends on the total H_2O content in the melts, which is at least in part because the H_2O/OH-ratio of hydrous melts increases with increasing water content (e.g., Stolper, 1982; Zotov and Keppler, 1998).

Additional details of the effect of melt polymerization (composition) and water content on melt speciation was addressed by calibrating band intensity from Raman spectra of the hydrous glass with ^{29}Si MAS NMR data from some of the samples. Calibration was carried out with hydrous NS8, NS4, NS2 2/3, and NS2 glasses with ~14 mol% H_2O (7.6–7.7 wt%). This is less than the water solubility in these melts under the conditions of these experiments (Mysen and Cody, 2004).

The integrated Raman intensities of the Raman bands assigned to Si-O^- vibrations in Q^2 and Q^3 species were calibrated in terms of mol fractions of these species via the simple expression

$$A_i/\sum A \cdot C = X_i \quad (1)$$

Here, A_i is the integrated intensity of Raman bands assigned to Si-O^- vibrations in species, i. For Q^2 and Q^3 species, these are the bands in 930–990 and 1060–1100 cm^{-1} frequency regimes as discussed above. The ΣA is sum of the integrated Raman bands assigned to the Si-O^- vibrations in Q^2 and Q^3 structural units plus that assigned to Si-O^o in Q^4 units (see above). The X_i is the mol fractions of the same species from the ^{29}Si MAS NMR spectra, and C is a calibration factor.

By applying this calibration to the Raman spectra of glasses with different water contents, the Q^n-abundance and degree of

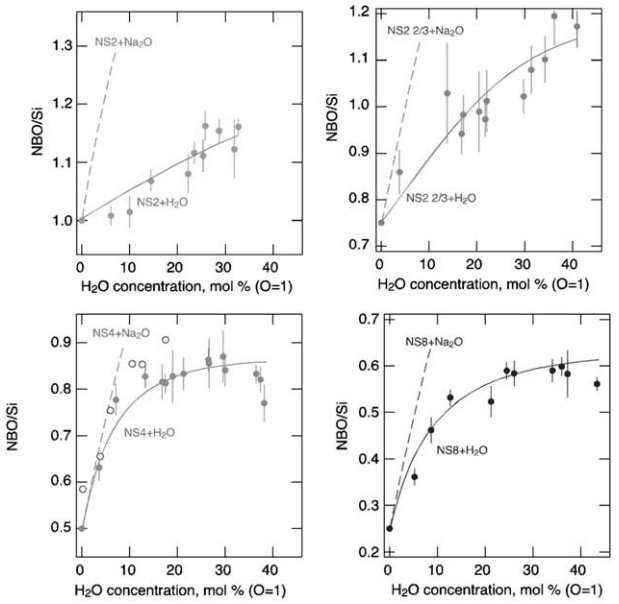

Fig. 5. Degree of polymerization, NBO/Si, of hydrous glasses a function of total H_2O content. Open symbols: data from Zotov and Keppler (998). Dashed lines: Degree of polymerization in anhydrous Na_2O-SiO_2 glasses as a function of Na_2O contents. Mol% calculated on the basis of O = 1. Data are from samples formed at 0.8–2.0 GPa and 1000°–1300°C. Error bars are calculated by progression of errors from the deconvolution of the Raman spectra and the error in the calibration factor, C (Eqn. 1). The latter error is obtained by progression of errors from deconvolution of the ^{29}Si MAS NMR spectra.

polymerization, NBO/Si, were calculated as a function of water content and Na/Si of the materials. In this calculation, it is assumed that for each of the silicate compositions, the calibration factor, C, is independent on water content. This assumption is considered reasonable because there is no evidence from the Raman spectra that the types of the Q^n species depend on total water content. The sum of the mol fractions of Q^n species containing nonbridging oxygen multiplied by the NBO/Si of the individual Q^n species, equals the degree of polymerization of the silicate, NBO/Si,

$$2 \times X_{Q2} + X_{Q3} = \mathrm{NBO/Si}, \tag{2}$$

where X_{Q2} and X_{Q3} are the mol fractions of Q^2 and Q^3, respectively.

The extent of depolymerization, expressed as their bulk NBO/Si, of all the quenched hydrous melts increases with increasing total water (Fig. 5). The 3. order polynomials fitted to the data points, constrained to pass through the NBO/Si of the anhydrous end member, do not have a physicochemical meaning. They are used simply to emphasize the trends in Figure 5.

The rate of NBO/Si-increase with water content is nonlinear and decreases with increasing total water. These relationships do not seem affected by the pressure and temperature at which the melts were formed.

The effect on bulk NBO/Si of adding equivalent concentrations of Na_2O to each of the Na_2O-SiO_2 glasses (dashed lines in Fig. 5) is greater than the effect of dissolved water. The difference between the two NBO/Si trajectories increases with increasing oxide (Na_2O and H_2O) concentration.

This difference between Na_2O and H_2O on their effect on NBO/Si of the melts, which suggests that Na_2O is a more effective depolymerizing agent than water, is in part because water most likely is dissolved both in molecular form (H_2O) and as OH-groups (e.g., Stolper, 1982; Silver et al., 1990; Zotov and Keppler, 1998; Sowerby and Keppler, 1999). Solution of molecular H_2O has no effect on the NBO/Si of the melt. When water is dissolved as OH groups, these may be either in the form of Si-OH or Na-OH complexes. Their existence and relative importance may affect the extent to which NBO/Si changes (Mysen and Virgo, 1986). Si-OH bonding is consistent with both ^{29}Si SPMAS NMR and Raman data. Furthermore, Cody et al. (2005) concluded that the resonance near 4 ppm in the ^{1}H SPMAS NMR spectra was consistent with protons in Na-OH complexes. Cody et al. (2005) noted that such complexes becomes more important the more sodic the glass.

The type of OH-complexing governs the extent of silicate melt polymerization resulting from dissolved water. Formation of Si-OH bonds may be viewed a simple depolymerization reaction conceptually similar to forming nonbridging oxygen upon solution of Na_2O:

$$\mathrm{Na_2O : Si\text{-}O\text{-}Si + Na_2O = 2Si\text{-}O\text{-}Na} \tag{3a}$$

$$\mathrm{H_2O : Si\text{-}O\text{-}Si + H_2O = 2Si\text{-}O\text{-}H.} \tag{3b}$$

In other words, in reactions 3a and 3b, one bridging oxygen, Si-O-Si, is converted to two nonbridging oxygen per Na^+ (Na-O-Si) or H^+ (H-O-Si).

Formation of Na-OH complexes may, however, affect the melt structure quite differently. Here, the Na^+ may be scavenged from its network-modifying role in anhydrous melts to form Na-OH complexes in hydrous melts. Schematically, such a mechanism would cause polymerization of the silicate network

$$\mathrm{2Si\text{-}O\text{-}Na + H_2O = 2NaOH + Si\text{-}O\text{-}Si} \tag{3c}$$

In Eqn. 3c, two nonbridging oxygen, Na-O-Si, are converted to one bridging oxygen, Si-O-Si, and 2 Na-OH bonds.

The relative importance of reactions 3a–c controls the extent to which dissolved water causes silicate polymerization. If the interpretation of the ^{1}H MAS NMR spectra by Cody et al. (2005) is correct, as the Na/Si increases, reaction 3c becomes increasingly important. This implies that the greater the Na/Si (the more depolymerized the anhydrous melt) the less effective is water as a melt depolymerizer.

The NBO/Si trajectory of hydrous NS4 glass as a function of total water content by Zotov and Keppler (1998) is also shown in Figure 5 (open circles). Their trend resembles that determined here for nominally the same composition (although the NBO/Si-value of their anhydrous NS4 melt is ~0.58 compared with ~0.5 for anhydrous NS4 melt in the present study; see Table 1). The present data suggest, however, a slightly smaller effect on NBO/Si for a given total water content (Fig. 5). One possible explanation for this difference is a different quenching rates of the Zotov and Keppler (1998) compared with our experiments. In our experiments, the quenching rate is ~100°C/s from experimental temperature to near the glass

transition. Zotov and Keppler (1998) reported that their samples quenched from experimental temperature (1100°C) to room temperature in 1–2 s. There may also be an effect of pressure although we did not observe any pressure effect on the NBO/Si trajectory from samples quenched in the 0.8–2 GPa range. All the Zotov and Keppler (1998) samples were quenched from 0.2 GPa.

The differences between the NBO/Si trajectories for H_2O and Na_2O in Figure 5 most likely results from combinations of the three types of water interactions with silicate illustrated with the formalized expressions in Eqns. 3a–c. The relative importance of these reactions depends on both Na/Si and on the total water content. In addition, increasing water content results in increasing proportion of molecular H_2O (Stolper, 1982; Zotov and Keppler, 1998), which is also qualitatively consistent with the decreasing rate of depolymerization with increasing water content seen in Figure 5.

Increasing proportion of molecular H_2O in the melt structure is not, however, a likely explanation for the observation that the effect of dissolved water on the NBO/Si also decreases with increasing Na/Si of the melts (Fig. 5) because existing data do not suggest a strong effect of silicate composition on OH/H_2O ratios in silicate melts (Scholze, 1956; Orlova, 1962; Bartholomew et al., 1980; Takata et al., 1981; Stolper, 1982; Silver et al., 1990). It is possible, however, that this difference could be related to competition between the two principal OH-forming reactions in Eqns. 3b and 3c.

Increasing water contents causes the abundance of the individual Q^n-species to vary in a way somewhat similar to the effect of adding Na_2O to the same compositions (Figs. 6–8). In detail there are, however, differences in Q^n-species abundance evolution with oxide content (Na_2O or H_2O) depending on the Na/Si of the melts. For the most polymerized starting materials (NS8, NS4, and NS2 2/3) solution of water results in a decrease in Q^4 abundance and an increase in Q^3 and Q^2. However, the rate of Q^4 decrease is less pronounced the less polymerized the anhydrous melt. For the most depolymerized composition, NS2, the concentration of Q^4 units actually increases as the water content increases. This trend differs from that of adding Na_2O to NS2, where the Q^4 abundance decreases (Fig. 6). All these trends are, however, also consistent with the ^{29}Si MAS NMR data (Table 1).

One possible depolymerization reaction that can explain the trends in Figure 5 involves consumption of Q^4 and formation of Q^2. This reaction may be illustrated with the expression

$$Q^4 + H_2O \Leftrightarrow Q^2(H), \quad (4)$$

where $Q^2(H)$ denotes Q^2 species formed by breaking Si-O-Si bridges originally in Q^4-species.

Eqn. 4 describes the general evolution of Q^2-abundance in the water-bearing Na_2O-SiO_2 melts (Fig. 7). For most of the water concentration range, the mol fraction of Q^2, X_{Q2}, increases with water content although there may be a maximum or a plateau for NS4 and NS8 composition melts somewhere between 20 and 40 mol% H_2O. This feature leads to the suggestion that there may be additional solution mechanisms involved at high water contents although the data are insufficient to identify this mechanism(s).

The Q^3 abundance with water content is more complex than

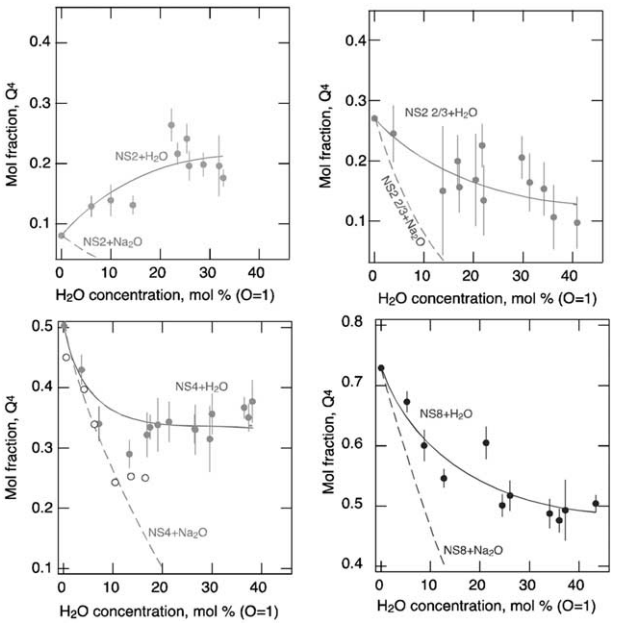

Fig. 6. Abundance of Q^4 species hydrous glasses a function of total H_2O content. Open symbols: data from Zotov and Keppler (998). Dashed lines: Abundance of Q^4 species in anhydrous Na_2O-SiO_2 glasses as a function of Na_2O contents (data from Maekawa et al., 1991). Mol% calculated on the basis of O = 1. Data are from samples formed at 0.8–2.0 GPa and 1000°–1300°C. Error bars are calculated by progression of errors from the deconvolution of the Raman spectra and the error in the calibration factor, C (Eqn. 1). The latter error is obtained by progression of errors from deconvolution of the ^{29}Si MAS NMR spectra.

for the other two species, Q^4 and Q^2 (Fig. 8). In the most polymerized melt composition, NS8, the X_{Q3} increases monotonously with water content. This behavior is most likely because both Q^3 and Q^2 species are formed as the result of interaction of H_2O with Si-O-Si bridges in Q^4 species as illustrated with Eqn. 4 and the equation

$$Q^4 + H_2O \Leftrightarrow Q^3(H). \quad (5)$$

For the less polymerized melt composition, NS4, the X_{Q3} passes through a maximum at a water concentration relatively similar to the Na_2O content corresponding to the X_{Q3} maximum of anhydrous melts on the join NS4-Na_2O (Fig. 8; see also Maekawa et al., 1991). The data by Zotov and Keppler (1998) for the join NS4-H_2O also show such a maximum (Fig. 8). This maximum most likely occurs because of at least two competing solution mechanisms for H_2O in the melt. One is the formation of $Q^3(H)$ species according to Eqn. 5. The other, which appears to dominate at higher water contents, probably involves interaction of dissolved water with Si-O-Si bridges in Q^3 species to form Q^2. This second mechanism,

$$Q^3 + H_2O \Leftrightarrow Q^2(H), \quad (6)$$

becomes increasingly important at decreasing water content the less polymerized (higher Na/Si) the melt (Fig. 8). In fact, for the two least polymerized melt composition, NS2 2/3 (NBO/Si = 0.75) and NS2 (NBO/Si = 1), the X_{Q3} always decreases. For NS2 2/3, the decrease is slight, whereas for NS2, the X_{Q3}

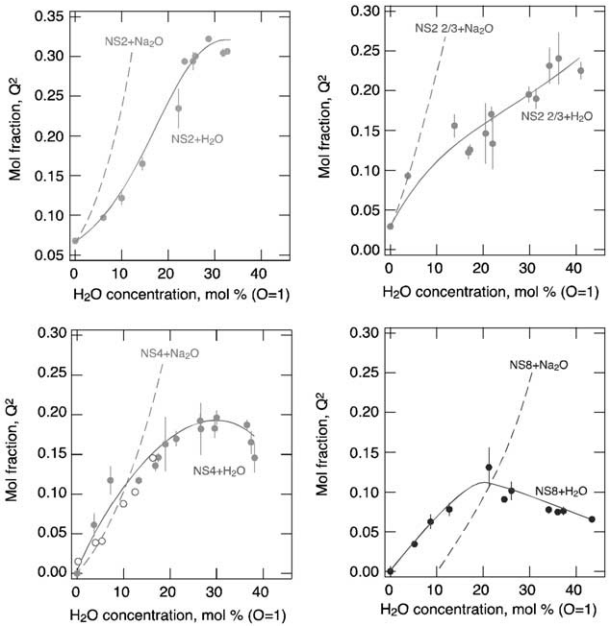

Fig. 7. Abundance of Q^2 species hydrous glasses a function of total H_2O content. Open symbols: data from Zotov and Keppler (1998). Dashed lines: Abundance of Q^2 species in anhydrous Na_2O-SiO_2 glasses as a function of Na_2O contents (data from Maekawa et al., 1991). Mol% calculated on the basis of O = 1. Data are from samples formed at 0.8–2.0 GPa and 1000°–1300°C. Error bars are calculated by progression of errors from the deconvolution of the Raman spectra and the error in the calibration factor, C (Eqn. 1). The latter error is obtained by progression of errors from deconvolution of the ^{29}Si MAS NMR spectra.

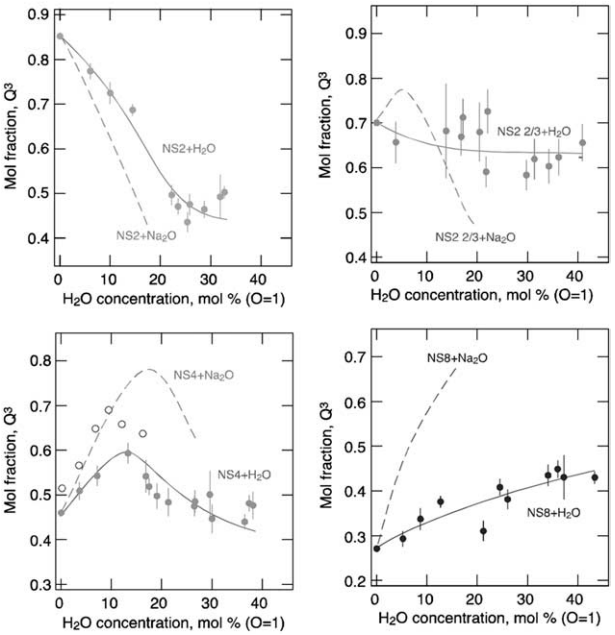

Fig. 8. Abundance of Q^3 species hydrous glasses a function of total H_2O content. Open symbols: data from Zotov and Keppler (998). Dashed lines: Abundance of Q^3 species in anhydrous Na_2O-SiO_2 glasses as a function of Na_2O contents (data from Maekawa et al., 1991). Mol% calculated on the basis of O = 1. Data are from samples formed at 0.8–2.0 GPa and 1000°–1300°C. Error bars are calculated by progression of errors from the deconvolution of the Raman spectra and the error in the calibration factor, C (Eqn. 1). The latter error is obtained by progression of errors from deconvolution of the ^{29}Si MAS NMR spectra.

decreases rapidly with increasing water content in the entire water concentration range investigated. This is because the mol fraction of Q^4, X_{Q4} is decreasingly important and X_{Q3} increasingly important as the melts become less polymerized (Table 1). Therefore, this interaction between dissolved water and Si-O-Si bridges in Q^4 species (Eqn. 5) becomes less important and interaction with Si-O-Si bridges in Q^3 species more important (Eqn. 6) the less polymerized the silicate melt.

Interestingly, regardless of Na/Si, the rate by which Q^4 is consumed and Q^3 and Q^2 species are formed, is not as pronounced as in melts to which is added equivalent proportions of a network-modifier such as Na^+ (Figs. 6–8). This difference is at least in part because some of the water in these melts most likely exists in molecular form.

However, those solution mechanisms alone cannot be reconciled with all aspects of Q^n abundance evolution, Na/Si, and water content of the melts. This conclusion brings up the possibility that Na-OH complexes may also be formed. The ^1H MAS NMR data of Cody et al. (2005) suggest that some Na^+ may also interact with water to form Na-OH complexes. There is also evidence for metal-OH complexing in other binary and ternary metal oxide silicate melts as reported recently by Xue and Kanzaki (2004).

Sodium-OH complexing is likely to become increasingly important as the Na/Si of the melts increases. Because Na-OH formation scavenges network-modifying Na^+ from the melt, this is, therefore, a reaction that causes polymerization of the silicate melt. Expressed in terms of changes in Q^n-speciation, we can in principle write an expression for this process as

$$4Q^3 + 2Na^+ + 2H_2O \Leftrightarrow 3Q^4 + Q^2 + 2NaOH + 2H^+ \quad (7)$$

Reaction 7 becomes increasingly dominant with increasing Na/Si so that in the system NS2+H_2O the NBO/Si of the melt hardly changes with water content (Fig. 5, Table 1).

If this trend continues to even less polymerized melts than NS2 (NBO/Si >1), it is possible that there exists a metal/silicon ratio above which solution of water actually results in polymerization of silicate melt. In addition, because the stability of metal-OH complexes is enhanced with increasing ionization potential of the metal cation (Xue and Kanzaki, 2004), one might speculate that the value of the metal/silicon ratio where silicate polymerization occurs decreases in the same direction. In this scenario, transition from depolymerization to polymerization of the silicate melt may occur at lower metal oxide/silicon ratio for alkaline earth than for alkali silicate melts.

From these relations, one might infer that water does not always cause depolymerization of partial melts in the interior of the Earth. In the deep upper mantle and below, partial melts formed under anhydrous conditions are ultramafic (e.g., Herzberg et al., 1990; Presnall and Gasparik, 1990; Herzberg and Zhang, 1997) with alkaline earths as the dominant network-modifying cations (Mysen, 1988). These melts are highly depolymerized with NBO/Si near 2 (e.g., Mysen, 1988). In light of the relationship between anhydrous melt polymerization and

rate of depolymerization with water discussed above, it is indeed possible that in the presence of water during partial melting in the upper mantle such partial melts might be more polymerized than melts formed under anhydrous conditions at similar conditions.

Increasing melt polymerization normally is also associated with increased silicate activity (e. g., Kushiro, 1975). Therefore, provided that the mineral assemblage in equilibrium with anhydrous and hydrous melts at the same depth in the mantle is the same, melts formed by wet partial melting is likely less silica-rich than those which may have formed under anhydrous conditions.

Acknowledgments—Critical reviews by Grant Henderson and two anonymous reviewers are appreciated. This research was conducted with partial support from NSF grant EAR-0405383

Associate editor: F. J. Ryerson

REFERENCES

Bartholomew R. F., Butler B. L., Hoover H. L., and Wu C.-K. (1980) Infrared spectra of water-containing glasses. *J. Am. Ceram. Soc.* **63,** 481–485.

Bell R. J. and Dean P. (1972) Localization of phonons in vitreous silica and related glasses. In *International Conference on the Physics of Non-Crystal Solids* (ed. R. W. D. Ellis), pp. 443–452. Wiley-Interscience.

Bohlen S. R. (1984) Equilibria for precise pressure calibration and a frictionless furnace assembly for the piston-cylinder apparatus. *N. Jb. Mineral. Mh.* **84,** 404–412.

Boyd F. R. and England J. L. (1960) Apparatus for phase equilibrium measurements at pressures up to 50 kilobars and temperatures up to 1750° C. *J. Geophys. Res.* **65,** 741–748.

Brawer S. A. and White W. B. (1975) Raman spectroscopic investigation of the structure of silicate glasses. I. The binary silicate glasses. *J. Chem. Phys.* **63,** 2421–2432.

Brawer S. A. and White W. B. (1977) Raman spectroscopic investigation of the structure of silicate glasses. II. The soda-alkaline earth-alumina ternary and Quaternary glasses. *J. Non-Cryst. Solids* **23,** 261–278.

Buckermann W.-A., Muller-Warmuth W., and Frischat G. H. (1992) A further ^{29}Si MAS NMR study on binary alkali silicate glasses. *Glasstechn. Ber.* **65,** 18–21.

Burnham C. W. (1975) Water and magmas; a mixing model. *Geochim. Cosmochim. Acta* **39,** 1077–1084.

Chekhmir A. S., Epel'baum M. B., and Simakin A. G. (1988) Water transport in magmas. *Geochem. Int.* **26,** 125–127.

Cody G. D., Mysen B. O., and Lee S. K. (2005) Structure vs. composition: A solid state ^{1}H and ^{29}Si NMR study of quenched glasses along the Na_2O-SiO_2-H_2O join. *Geochim. Cosmochim. Acta* **69,** 2373–2384,

Engelhardt G. and Michel D. (1987) *High-Resolution Solid-State NMR of Silicates and Zeolites.* Wiley.

Farnan I., Kohn S. C., and Dupree R. (1987) A study of the structural role of water in hydrous silica using cross-polarisation magic angle NMR. *Geochim. Cosmochim. Acta* **51,** 2869–2874.

Fukumi K., Hayakawa J., and Komiyama T. (1990) Intensity of Raman band in silicate glasses. *J. Non-Cryst. Solids* **119,** 297–302.

Furukawa T., Fox K. E., and White W. B. (1981) Raman spectroscopic investigation of the structure of silicate glasses. III. Raman intensities and structural units in sodium silicate glasses. *J. Chem. Phys.* **153,** 3226–3237.

Herzberg C. and Zhang J. (1997) Melting experiments on komatiite analog compositions at 5 GPa. *Am. Mineral.* **82,** 354–367.

Herzberg C., Gasparik T., and Sawamoto H. (1990) Origin of mantle peridotite: Contraints from melting experiments to 16.5 GPa. *J. Geophys. Res.* **95,** 15779–15805.

Hess K.-U. and Dingwell D. B. (1996) Viscosities of hydrous leucogranitic melts: A non-Ahrrenian model. *Am. Mineral.* **81,** 1297–1300.

Kohn S. C., Dupree R., and Mortuza M. G. (1992) The interaction between water and aluminosilicate magma. *Chem. Geol.* **96,** 399–410.

Kümmerlen J., Merwin L. H., Sebald A., and Keppler H. (1992) Structural role of H_2O in sodium silicate glasses: Results from ^{29}Si and ^{1}H NMR spectroscopy. *J. Phys. Chem.* **96,** 64–56410.

Kushiro I. (1975) On the nature of silicate melt and its significance in magma genesis: Regularities in the shift of liquidus boundaries involving olivine pyroxene and silica materials. *Am. J. Sci.* **275,** 411–431.

Kushiro I. (1976) A new furnace assembly with a small temperature gradient in solid-media, high-pressure apparatus. *Carnegie Inst. Wash. Year Book* **75,** 832–833.

Lasaga A. C. (1982) Optimization of CNDO for molecular orbital calculation on silicates. *Phys. Chem. Minerals* **8,** 36–46.

Long D. A. (1977) *Raman Spectroscopy.* McGraw-Hill.

Maekawa H., Maekawa T., Kawamura K., and Yokokawa T. (1991) The structural groups of alkali silicate glasses determined from ^{29}Si MAS-NMR. *J. Non-Cryst. Solids* **127,** 53–64.

Mao H. K., Bell P. M., and England J. L. (1971) Tensional errors and drift of the thermocouple electromotive force in the single stage, piston-cylinder apparatus. *Carnegie Inst. Wash. Year Book* **70,** 281–287.

McMillan P. (1984) Structural studies of silicate glasses and melts—Applications and limitations of Raman spectroscopy. *Am. Mineral.* **69,** 622–644.

McMillan P. F. and Remmele R. L. (1986) Hydroxyl sites in SiO_2 glass: A note on infrared and Raman spectra. *Am. Mineral.* **71,** 772–778.

McMillan P. F., Wolf G. H., and Poe B. T. (1992) Vibrational spectroscopy of silicate liquids and glasses. *Chem. Geol.* **96,** 351–366.

McMillan P. F. and Wolf G. H. (1995) Vibrational spectroscopy of silicate liquids. In *Structure, Dynamics and Properties of Silicate Melts* (eds. J. F. Stebbins, P. F. McMillan and D. B. Dingwell), pp. 247–315. Mineralogical Society of Washington.

Moulson A. J. and Roberts J. P. (1961) Water in silica glass. *Trans. Faraday Soc.* **57,** 1208–1216.

Mysen B. O. (1988) *Structure and Properties of Silicate Melts.* Elsevier.

Mysen B. O. (1995) Experimental, in-situ, high-temperature studies of properties and structure of silicate melts relevant to magmatic temperatures. *Eur. J. Mineral.* **7,** 745–766.

Mysen B. O. (2003) Physics and chemistry of silicate glasses and melts. *Eur. J. Mineral.* **15,** 781–802.

Mysen B. O., Virgo D., and Seifert F. A. (1982) The structure of silicate melts: Implications for chemical and physical properties of natural magma. *Rev. Geophys.* **20,** 353–383.

Mysen B. O. and Virgo D. (1986) Volatiles in silicate melts at high pressure and temperature. 1. Interaction between OH groups and Si^{4+}, Al^{3+}, Ca^{2+}, Na^{+} and H^{+}. *Chem. Geol.* **57,** 303–331.

Mysen B. O. and Frantz J. D. (1994) Structure of haplobasaltic liquids at magmatic temperatures: In-situ, high-temperature study of melts on the join $Na_2Si_2O_5$-$Na_2(NaAl)_2O_5$. *Geochim. Cosmochim. Acta* **58,** 1711–1733.

Mysen B. O. and Wheeler K. (2000) Solubility behavior of water in haploandesitic melts at high pressure and high temperature. *Am. Mineral.* **85,** 1128–1142.

Mysen B. O. and Cody G. D. (2004) Solubility and solution mechanism of H_2O in alkali silicate melts and glasses at high pressure and temperature. *Geochem. Cosmochim. Acta* **68,** 5113–5126.

Nowak M. and Behrens H. (1995) The speciation of water in haplogranitic glasses and melts by in-situ, near-infrared spectroscopy. *Geochim. Cosmochim. Acta* **59,** 3445–3450.

Orlova G. P. (1962) The solubility of water in albite melt. *Int. Geol. Rev.* **6,** 254–258.

Osborn E. F. and Muan A. (1960) Phase equilibrium diagrams for ceramists, plate 4: The system Na_2O-Al_2O_3-SiO_2. American Ceramics Society.

Padro D., Schmidt B. C., and Dupree R. (2003) Water solubility mechanism in hydrous aluminosilicate glass: Information from ^{27}Al

MAS and MQMAS NMR. *Geochim. Cosmochim. Acta* **67,** 1543–1552.

Presnall D. C. and Gasparik T. (1990) Melting of enstatite ($MgSiO_3$) from 10 to 16.5 GPa and the forsterite (Mg_2SiO_4)-majorite ($MgSiO_3$) eutectic at 16.5 GPa: Implications for the origin of the mantle. *J. Geophys. Res.* **95,** 15771–15778.

Revesz A. G. and Walrafen G. E. (1983) Structural interpretation of some of the Raman lines from vitreous silica. *J. Non-Cryst. Solids* **54,** 323–355.

Schaller T. and Sebald A. (1995) One- and two-dimensional ^{1}H magic-angle spinning experiments on hydrous silicate glasses. *Solid State Nucl. Magn. Resonance* **5,** 89–102.

Schmidt B. C., Riemer T., Kohn S. C., Holtz F., and Dupree R. (2001) Structural implications of water dissolution in haplogranitic glasses from NMR spectroscopy: Influence of total water content and mixed alkali effect. *Geochim. Cosmochim. Acta* **65,** 2949–2964.

Scholze H. (1956) Der Einbau des Wassers in Glasern. *Int. Congress Glass* **4,** 424–429.

Silver L., Ihinger P. D., and Stolper E. (1990) The influence of bulk composition on the speciation of water in silicate glasses. *Contrib. Mineral. Petrol.* **104,** 142–162.

Sowerby J. R. and Keppler H. (1999) Water speciation in rhyolitic melt determined by in-situ infrared spectroscopy. *Am. Mineral.* **84,** 1843–1849.

Stebbins J. F. (1987) Identification of multiple structural species in silicate glasses by ^{29}Si NMR. *Nature* **330,** 465–467.

Stebbins J. F. (1995) Dynamics and structure of silicate and oxide melts; nuclear magnetic resonance studies. In *Structure, Dynamics and Properties of Silicate Melts*, Vol. 32 (eds. J. F. Stebbins, P. F. McMillan and D. B. Dingwell), pp. 191–246. Mineralogical Society of America.

Stolen R. H. and Walrafen G. E. (1976) Water and its relation to broken bond defects in fused silica. *J. Chem. Phys.* **64,** 2623–2631.

Stolper E. (1982) The speciation of water in silicate melts. *Geochim. Cosmochim. Acta* **46,** 2609–2620.

Takata M., Acocella J., Tomozawa M., and Watson E. B. (1981) Effect of water content on the electrical conductivity of $Na_2O \cdot 3SiO_2$ glass. *J. Am. Ceram. Soc.* **64,** 719–724.

Wasserburg G. J. (1957) The effects of H_2O in silicate systems. *J. Geol.* **65,** 15–23.

Watson E. B. (1994) Diffusion in volatile-bearing magmas. In *Volatiles in Magmas* (eds. M. R. Carroll and J. R. Holloway), pp. 371–411. Mineralogical Society of America.

Xue Y. and Kanzaki M. (2004) Dissolution mechanisms of water in depolymerized silicate melts: Constraints from ^{1}H and ^{29}Si NMR spectroscopy and ab initio calculations. *Geochim. Cosmochim. Acta* **68,** 5027–5058.

Zhang Y., Stolper E. M., and Wasserburg G. J. (1991) Diffusion of water in rhyolitic glasses. *Geochim. Cosmochim. Acta* **55,** 441–456.

Zotov N. and Keppler H. (1998) The influence of water on the structure of hydrous sodium tetrasilicate glasses. *Am. Mineral.* **83,** 823–834.